THE ASTROPHYSICAL JOURNAL, 554:615–623, 2001 June 10
© 2001. The American Astronomical Society. All rights reserved. Printed in U.S.A.

RADIATIVE EQUILIBRIUM AND TEMPERATURE CORRECTION IN MONTE CARLO RADIATION TRANSFER

J. E. BJORKMAN
Ritter Observatory, Department of Physics and Astronomy, University of Toledo, Toledo, OH 43606-3390; jon@astro.utoledo.edu
AND
KENNETH WOOD
Harvard-Smithsonian Center for Astrophysics, 60 Garden Street, Cambridge, MA 02138; kwood@cfa.harvard.edu
Received 2000 November 15; accepted 2001 February 13

ABSTRACT

We describe a general radiative equilibrium and temperature correction procedure for use in Monte Carlo radiation transfer codes with sources of temperature-independent opacity, such as astrophysical dust. The technique utilizes the fact that Monte Carlo simulations track individual photon packets, so we may easily determine where their energy is absorbed. When a packet is absorbed, it heats a particular cell within the envelope, raising its temperature. To enforce radiative equilibrium, the absorbed packet is immediately reemitted. To correct the cell temperature, the frequency of the reemitted packet is chosen so that it corrects the temperature of the spectrum previously emitted by the cell. The reemitted packet then continues being scattered, absorbed, and reemitted until it finally escapes from the envelope. As the simulation runs, the envelope heats up, and the emergent spectral energy distribution (SED) relaxes to its equilibrium value *without iteration.* This implies that the equilibrium temperature calculation requires no more computation time than the SED calculation of an equivalent pure scattering model with fixed temperature. In addition to avoiding iteration, our method conserves energy exactly because all injected photon packets eventually escape. Furthermore, individual packets transport energy across the entire system because they are never destroyed. This long-range communication, coupled with the lack of iteration, implies that our method does not suffer the convergence problems commonly associated with Λ-iteration. To verify our temperature correction procedure, we compare our results with standard benchmark tests, and finally we present the results of simulations for two-dimensional axisymmetric density structures.

Subject headings: circumstellar matter — dust, extinction — radiative transfer — scattering

1. INTRODUCTION

There is an ever increasing wealth of observational evidence indicating the nonsphericity of almost every type of astronomical object (e.g., extended circumstellar environments, novae shells, planetary nebulae, galaxies, and active galactic nuclei). To interpret this data accurately, detailed two- and three-dimensional radiation transfer techniques are required. With the availability of fast workstations, many researchers are turning to Monte Carlo techniques to produce model images and spectra for the asymmetric objects they are investigating. In Monte Carlo radiation transfer simulations, packets of energy or "photons" are followed as they are scattered and absorbed within a prescribed medium. One of the features of this technique is that the locations of the packets are known when they are absorbed, so we can determine where their energy is deposited. This energy heats the medium, and to conserve radiative equilibrium, the absorbed energy must be reradiated at other wavelengths, depending on the opacity sources present. Tracking these photon packets, while enforcing radiative equilibrium, permits the calculation of both the temperature structure and the emergent spectral energy distribution (SED) of the envelope. The ability of Monte Carlo techniques to easily follow the transfer of radiation through complex geometries makes them very attractive methods for determining the temperature structure within nonspherical environments—a task that is very difficult with traditional ray-tracing techniques.

Previous work on this problem for spherical geometries includes the approximate solutions by Scoville & Kwan (1976), who ignored scattering, and Leung (1976), and the diffusion approximations by Yorke (1980). The spherically symmetric problem has been solved exactly by Rowan-Robinson (1980), Wolfire & Cassinelli (1986), and Ivezić & Elitzur (1997), who used a scaling technique. Extensions of the exact solution to two dimensions have been performed by Efstathiou & Rowan-Robinson (1990, 1991), while approximate two-dimensional models have been presented by Sonnhalter, Preibisch, & Yorke (1995) and Men'shchikov & Henning (1997).

Radiative equilibrium calculations using the Monte Carlo technique have been presented by Lefevre, Bergeat, & Daniel (1982), Lefevre, Daniel, & Bergeat (1983), Wolf, Henning, & Secklum (1999), and Lucy (1999). Most of these authors (Lucy being exceptional) use a technique in which stellar and envelope photon packets are emitted separately. The number of envelope packets to be emitted is determined by the envelope temperature, while the envelope temperature is determined by the number of absorbed packets. Consequently, these techniques require iteration, usually using the absorbed stellar photons to provide an initial guess for the envelope temperature. The iteration proceeds until the envelope temperatures converge. Note that the stellar luminosity is not automatically conserved during the simulation; only after the temperatures converge is the luminosity approximately conserved.

In contrast, Lucy adopts a strategy in which absorbed photon packets are immediately reemitted, using a frequency distribution set by the current envelope temperature. Although the frequency distribution of the

reprocessed photons is incorrect (until the temperatures have converged), his method automatically enforces local radiative equilibrium and implicitly conserves the stellar luminosity. The insight of Lucy's method is that conservation of the stellar luminosity is more important than the SED when calculating the radiative equilibrium temperatures. Nonetheless, this method requires iteration.

The primary problem faced by Lucy's method is the incorrect frequency distribution of the reemitted photons. In this paper we develop an adaptive Monte Carlo technique that corrects the frequency distribution of the reemitted photons. Essentially, our method relaxes to the correct frequency and temperature distribution. Furthermore, it requires no iteration as long as the opacity is independent of temperature. Such is the case for astrophysical dust. In § 2, we describe the temperature correction algorithm. We compare the results of our code with a spherically symmetric code in § 3, and in § 4 we present results for two-dimensional axisymmetric density structures.

2. MONTE CARLO RADIATIVE EQUILIBRIUM

We wish to develop a method to calculate the temperature distribution throughout an extended dusty environment for use with Monte Carlo simulations of the radiation transfer. The radiation transfer technique we employ has been described in detail in other papers (Code & Whitney 1995; Whitney & Hartmann 1992, 1993; Wood et al. 1996), so we only summarize it here. The basic idea is to divide the luminosity of the radiation source into equal-energy, monochromatic "photon packets" that are emitted stochastically by the source. These packets are followed to random interaction locations, determined by the optical depth, where they are either scattered or absorbed with a probability given by the albedo. If the packet is scattered, a random scattering angle is obtained from the scattering phase function (differential cross section). If instead the packet is absorbed, its energy is added to the envelope, raising the local temperature. To conserve energy and enforce radiative equilibrium, the packet is reemitted immediately at a new frequency determined by the envelope temperature. These reemitted photons comprise the diffuse radiation field. After either scattering or absorption plus reemission, the photon packet continues to a new interaction location. This process is repeated until all the packets escape the dusty environment, whereupon they are placed into frequency and direction-of-observation bins that provide the emergent SED. Since all the injected packets eventually escape (either by scattering or absorption followed by reemission), this method implicitly conserves the total energy. Furthermore, it automatically includes the diffuse radiation field when calculating both the temperature structure and the emergent SED.

We now describe in detail how we calculate the temperature structure and SEDs of dusty environments illuminated by a radiation source. This radiation can come from any astrophysical source, either internal or external, point-like or extended.

2.1. *Radiative Equilibrium Temperature*

Initially, we divide the source luminosity L into N_γ photon packets emitted over a time interval Δt. Each photon packet has the same energy E_γ, so

$$E_\gamma = L\Delta t/N_\gamma \,. \tag{1}$$

Note that the number of physical photons in each packet is frequency-dependent.

When the monochromatic photon packet is injected into the envelope, it will be assigned a random frequency chosen from the SED of the source. This frequency determines the dust absorptive opacity κ_ν and scattering opacity σ_ν (both per mass), as well as the scattering parameters for the ensuing random walk of the packet through the envelope. The envelope is divided into spatial grid cells with volume V_i, where i is the cell index. As we inject source photon packets, we maintain a running total N_i of how many packets are absorbed in each grid cell. Whenever a packet is absorbed in a grid cell, we deposit its energy in the cell and recalculate the cell's temperature. The total energy absorbed in the cell

$$E_i^{\rm abs} = N_i E_\gamma \,. \tag{2}$$

We assume that the dust particles are in local thermodynamic equilibrium (LTE), and for simplicity, we adopt a single temperature for the dust grains. Note that although we use dust for the continuous opacity source, we could replace the dust with any continuous LTE opacity source that is independent of temperature. In radiative equilibrium, the absorbed energy $E_i^{\rm abs}$ must be reradiated. The thermal emissivity of the dust $j_\nu = \kappa_\nu \rho B_\nu(T)$, where $B_\nu(T)$ is the Planck function at temperature T, so the emitted energy is

$$E_i^{\rm em} = 4\pi\Delta t \int dV_i \int \rho\kappa_\nu B_\nu(T)\, d\nu \tag{3}$$

$$= 4\pi\Delta t \int \kappa_{\rm P}(T) B(T) \rho\, dV_i \,, \tag{4}$$

where $\kappa_{\rm P} = \int \kappa_\nu B_\nu d\nu / B$ is the Planck mean opacity and $B = \sigma T^4/\pi$ is the frequency integrated Planck function. If we adopt a temperature that is constant throughout the grid cell, T_i, then

$$E_i^{\rm em} = 4\pi\Delta t \kappa_{\rm P}(T_i) B(T_i) m_i \,, \tag{5}$$

where m_i is the mass of the cell.

Equating the absorbed (eq. [2]) and emitted (eq. [5]) energies, we find that after absorbing N_i packets, the dust temperature is given by

$$\sigma T_i^4 = \frac{N_i L}{4 N_\gamma \kappa_{\rm P}(T_i) m_i} \,. \tag{6}$$

Note that the Planck mean opacity $\kappa_{\rm P}$ is a function of temperature, so equation (6) is actually an implicit equation for the temperature, which must be solved *every time a packet is absorbed*. Since this equation is solved so many times, an efficient algorithm is desirable. Fortunately, $\kappa_{\rm P}$ is a slowly varying function of temperature, which implies a simple iterative algorithm may be used to solve equation (6). To do so efficiently, we pretabulate the Planck mean opacities for a large range of temperatures and evaluate $\kappa_{\rm P}(T_i)$ by interpolation, using the temperature from the previous guess. After a few steps, we have the solution for T_i. Note that because the dust opacity is temperature-independent, the product $\kappa_i \sigma T_i^4$, which is proportional to $\int \kappa_\nu B_\nu d\nu$, increases monotonically with temperature. Consequently, T_i always increases when the cell absorbs an additional packet.

2.2. *Temperature Correction*

Now that we know the temperature after absorbing an additional packet within the cell, we must reradiate this

energy so that the heating always balances the cooling. Prior to absorbing this packet, the cell has emitted packets that carried away an energy corresponding to the cell's previous emissivity $j'_\nu = \kappa_\nu B_\nu(T_i - \Delta T)$, where ΔT is the temperature increase arising from the packet absorption. Note that these previous packets were emitted with an incorrect frequency distribution corresponding to the previous temperature, $T_i - \Delta T$. The total energy that should be radiated now corresponds to j_ν at the new temperature, T_i. Thus, the additional energy to be carried away is given by

$$\Delta j_\nu = j_\nu - j'_\nu = \kappa_\nu[B_\nu(T_i) - B_\nu(T_i - \Delta T)] , \quad (7)$$

which is the shaded area shown in Figure 1. As long as the packet energy E_γ is not too large (this may be assured by choosing a large enough number of photon packets, N_γ, to use for the simulation), the temperature change ΔT is small, so the temperature correction spectrum

$$\Delta j_\nu \approx \kappa_\nu \Delta T(dB_\nu/dT) . \quad (8)$$

Note that Δj_ν is everywhere positive because $\Delta T > 0$ and that the Planck function is a monotonically increasing function of temperature. Therefore, to correct the previously emitted spectrum, we immediately reemit the packet (to conserve energy), and we choose its frequency using the shape of Δj_ν. This procedure statistically reproduces Δj_ν for the distribution of the reemitted packets. Normalizing this distribution, we find the temperature correction probability distribution

$$\frac{dP_i}{d\nu} = \frac{\kappa_\nu}{K}\left(\frac{dB_\nu}{dT}\right)_{T=T_i} , \quad (9)$$

where $dP_i/d\nu$ is the probability of reemitting the packet between frequencies ν and $\nu + d\nu$, and the normalization constant $K = \int_0^\infty \kappa_\nu(dB_\nu/dT)d\nu$.

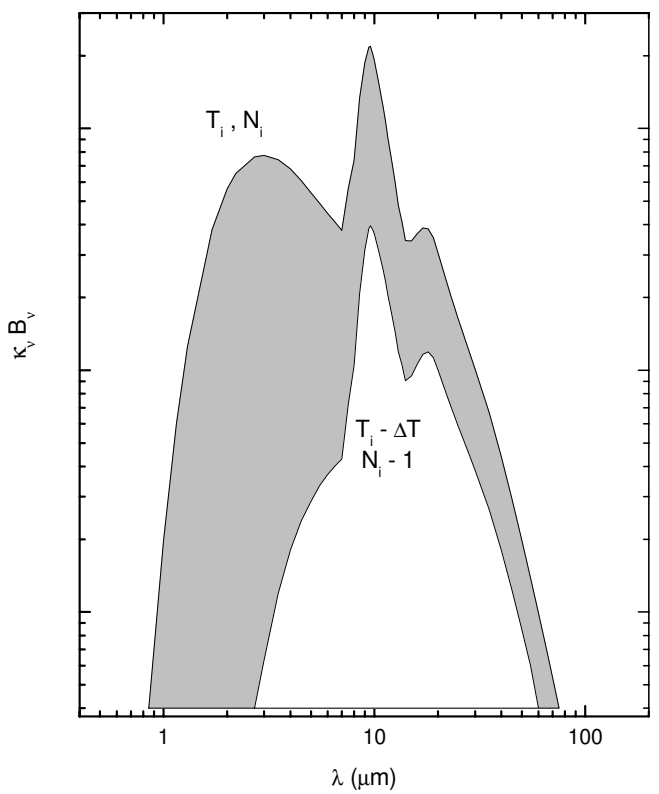

FIG. 1.—Temperature correction frequency distribution. Shown are the dust emissivities, $j_\nu = \kappa_\nu B_\nu(T)$, prior to and after the absorption of a single photon packet. The spectrum of the previously emitted packets is given by the emissivity at the old cell temperature (*bottom curve*). To correct the spectrum from the old temperature to the new temperature (*upper curve*), the photon packet should be reemitted using the difference spectrum (*shaded area*).

Now that the packet's frequency has changed, we change the opacity and scattering parameters accordingly and continue with scattering, absorption, temperature correction, and reemission until all the photon packets finally escape from the system. In principle, we could also account for the back-warming of the source. Whenever a packet hits the source, the source must reradiate this new energy. This will change the temperature of the source, and the new source photons can be emitted using a difference spectrum similar to equation (9).

When we begin our calculation, no packets have been absorbed, so the initial temperature is zero throughout the envelope. This means that the initial temperature change is not small, as is required by equation (8). One could use equation (7) to reemit the first packet that is absorbed; however, this is not necessary. The number of packets producing this initial temperature change is small; it is on the order of the number of spatial grid cells. Furthermore, these packets generally are reemitted at such long wavelengths that they are not observable. Consequently, the error arising from using equation (8) to reemit every packet is too small to be of importance.

As the simulation runs, the envelope starts at zero temperature. It then heats up, and the radiation field "relaxes" to its final spectral shape. The temperature correction procedure is simply a way of reordering the calculation (the frequencies that are being used at a given moment) so that in the end, all the frequencies have been properly sampled. Consequently, after all the stellar photon packets have been transported, the final envelope temperature is the correct radiative equilibrium temperature, and the emergent SED has the correct frequency shape. Furthermore, the photon reemission automatically accounts for the diffuse envelope emission. Note that energy is necessarily conserved, and there is no time-consuming iteration in our scheme; calculating the radiative equilibrium temperature requires no more computational time than an equivalent pure scattering calculation in which the temperature structure is held fixed. Similarly, there is no issue of convergence in our method. Unlike Λ-iteration, the photon packets carry energy over large distances throughout the envelope because they are never destroyed, and of course there is no iteration at all. After running N_γ packets, we have the final answer. The simulation does not continue running until some convergence criterion is met, and the only source of error in the calculation is the statistical sampling error inherent in Monte Carlo simulations.

3. BENCHMARK VERIFICATION

To validate our method for determining the radiative equilibrium temperatures and emergent fluxes, we compared our results against a set of benchmark calculations recently developed by Ivezić et al. (1997) for testing spherically symmetric dust radiative equilibrium codes. The parameters listed by Ivezić et al. enable us to reproduce exactly the same set of physical conditions (i.e., input spec-

trum, dust destruction radius, optical depth, opacity frequency distribution, and radial density structure).

For all benchmark tests, Ivezić et al. used a point-source star, radiating with a blackbody spectrum whose temperature $T_* = 2500$ K. The dust density distribution was a power law with radius

$$\rho = \rho_0 (R_{\rm dust}/r)^p \,, \tag{10}$$

where

$$\rho_0 = \frac{\tau_\lambda}{(\kappa_\lambda + \sigma_\lambda)(1 - R_{\rm dust}/R_{\rm max})} \begin{cases} 1/R_{\rm max} & (p = 0) \,, \\ 1/R_{\rm dust} & (p = 2) \,. \end{cases} \tag{11}$$

The inner radius of the envelope is the dust destruction radius $R_{\rm dust}$, the outer radius is $R_{\rm max}$, and the total radial optical depth is τ_λ, specified at $\lambda = 1$ μm. The dust absorptive opacity κ_ν and scattering opacity σ_ν were taken to be

$$\frac{\kappa_\nu}{(\kappa_{1\ \mu{\rm m}} + \sigma_{1\ \mu{\rm m}})} = 0.5 \begin{cases} 1 & (\lambda < 1\ \mu{\rm m}) \,, \\ (1\ \mu{\rm m}/\lambda) & (\lambda > 1\ \mu{\rm m}) \,, \end{cases} \tag{12}$$

$$\frac{\sigma_\nu}{(\kappa_{1\ \mu{\rm m}} + \sigma_{1\ \mu{\rm m}})} = 0.5 \begin{cases} 1 & (\lambda < 1\ \mu{\rm m}) \,, \\ (1\ \mu{\rm m}/\lambda)^4 & (\lambda > 1\ \mu{\rm m}) \,. \end{cases} \tag{13}$$

Since the total optical depth at 1 μm is independently specified, these opacities have been normalized to that at 1 μm for convenience. The wavelength-dependent scattering albedo is given by $a = \sigma_\nu/(\kappa_\nu + \sigma_\nu)$, and the scattering was assumed to be isotropic (note that in dust simulations, we would normally use a nonisotropic phase function for the scattering).

In principle, the inner radius of the dust shell $R_{\rm dust}$ is determined by the dust condensation temperature, chosen by Ivezić et al. to be $T_{\rm cond} = 800$ K. However, we are only testing the temperature correction procedure, so we have not implemented a scheme to solve self-consistently for the dust destruction radius. The values for $R_{\rm dust}$ were calculated instead using Ivezić et al.'s equation (4) and data from their Table 1. Finally, the outer radius of the dust shell was set to be $R_{\rm max} = 10^3 R_{\rm dust}$. The parameters describing the various test simulations are summarized in Table 1.

To begin the simulation, we release stellar photon packets with a blackbody frequency distribution, given by the normalized Planck function

$$b_\nu(x) = \frac{15}{\pi^4} \frac{x^3}{e^x - 1} \,, \tag{14}$$

where $x = h\nu/kT_*$. A particularly simple method for sampling the blackbody distribution is given by Carter & Cashwell (1975). Since this reference is somewhat obscure and difficult to obtain, we summarize the method here. First, generate a uniform random number ξ_0 in the range 0–1, and determine the minimum value of l, $l_{\rm min}$ that satisfies the condition

$$\sum_{i=1}^{l} i^{-4} \geq \frac{\pi^4}{90} \xi_0 \,. \tag{15}$$

Next, obtain four additional uniform random numbers (in the range 0–1), ξ_1, ξ_2, ξ_3, and ξ_4. Finally, the packet frequency is given by

$$x = -\ln(\xi_1 \xi_2 \xi_3 \xi_4)/l_{\rm min} \,. \tag{16}$$

After emitting these packets from the star, we track them through the envelope. To determine the envelope temperature, we must count how many packets are absorbed in each grid cell. Since the envelope is spherically symmetric, we employ a set of spherical shells for our grid. To obtain the best Poisson error statistics, we should ideally construct the grid positions so that equal numbers of packets are absorbed in each cell. Since the probability of absorbing a photon packet is proportional to the optical depth, we choose equal radial optical depth grid locations,

$$\frac{r_i}{R_{\rm dust}} = \begin{cases} i\Delta r + 1 & (p = 0) \,, \\ N_f/(N_f - i) & (p = 2) \,, \end{cases} \tag{17}$$

where $N_r = 200$ is the total number of cells we used, $\Delta r = (R_{\rm max}/R_{\rm dust} - 1)/N_r$, and $N_f = N_r/(1 - R_{\rm dust}/R_{\rm max})$. Integrating the density, equation (10), over the cell volume to obtain the mass, we find from equation (6) that the temperature in each grid cell is given by

$$T_i^4 = T_*^4 \,,$$

$$\begin{cases} \dfrac{N_i N_r (R_*/R_{\rm dust})^2 [(\kappa_{1\ \mu{\rm m}} + \sigma_{1\ \mu{\rm m}})/\kappa_{\rm P}(T_i)]}{4 N_\gamma \tau_{1\ \mu{\rm m}} [(i^2 - i + 1/3)\Delta r^2 + (2i - 1)\Delta r + 1]} & (p = 0) \,, \\ \dfrac{N_i (N_f - i)(N_f - i + 1)(R_*/R_{\rm dust})^2 (1 - R_{\rm dust}/R_{\rm max})}{4 N_\gamma \tau_{1\ \mu{\rm m}} N_f [\kappa_{\rm P}(T_i)/(\kappa_{1\ \mu{\rm m}} + \sigma_{1\ \mu{\rm m}})]} & (p = 2) \,, \end{cases} \tag{18}$$

where we have used $L = 4\pi R_*^2 \sigma T_*^4$ for the stellar luminosity.

We then proceed with the radiation transfer, temperature calculation, and reemission as described in § 2 until all packets exit the envelope. When the packets escape, they are placed into $N_\nu = 1024$ uniform frequency bins,

$$\nu_k = \nu_{\rm max} \frac{k}{N_\nu} \,, \tag{19}$$

where $h\nu_{\rm max} = 16 kT_*$. The width of each bin $\Delta\nu = \nu_{\rm max}/N_\nu$. Since the envelope is spherically symmetric, the observed flux $F_{\nu_k} = N_k E_\gamma / 4\pi d^2 \Delta t \Delta\nu$, where N_k is the number of packets in the kth frequency bin and d is the observer's distance from the star. Normalizing to the total flux, $F = L/4\pi d^2$, the SED is given by

$$\left(\frac{\nu F_\nu}{F}\right)_k = (k - 1/2) \frac{N_k}{N_\gamma} \,. \tag{20}$$

The factor $(k - 1/2)$ arises from using the frequency at the center of the bin.

In Figures 2*a* and 2*b* we show the results of our simulation compared with the output of one of the codes tested by

TABLE 1

SPHERICAL MODELS

$\tau_{1\ \mu{\rm m}}$	$R_{\rm dust}/R_*$
$p = 0$	
1	8.44
10	8.46
100.....	8.60
$p = 2$	
1	9.11
10	11.37
100.....	17.67

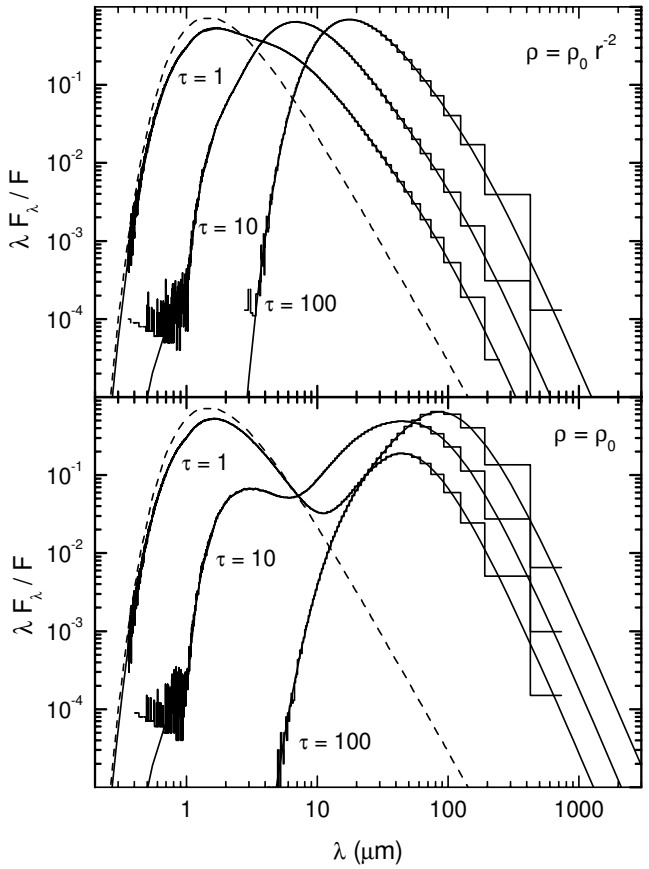

FIG. 2*a*

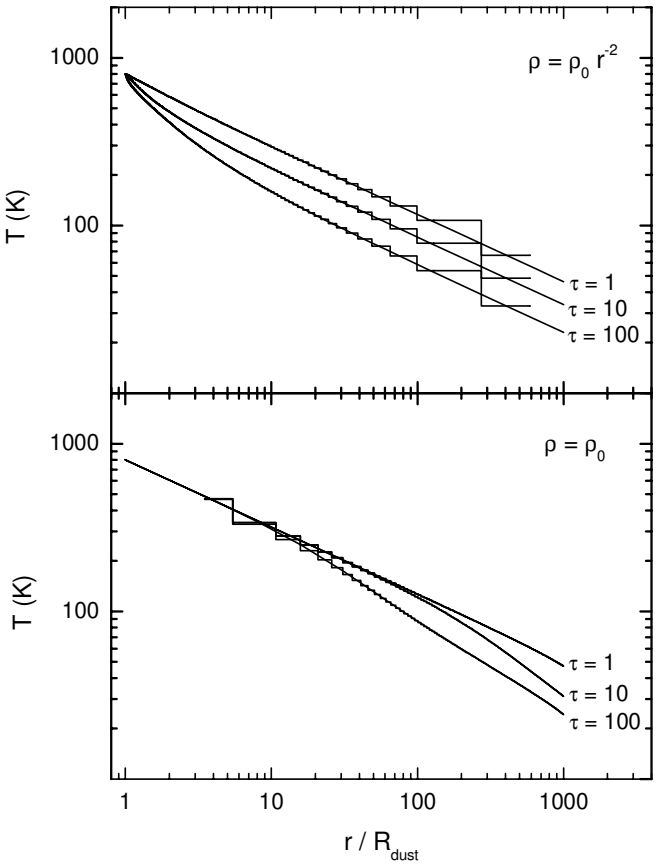

FIG. 2*b*

FIG. 2.—(*a*) Spherical model SEDs. Shown are the comparisons of our spherically symmetric model fluxes (*histogram*) with those from DUSTY (*solid curves*). The top panel compares the $1/r^2$ density models, while the bottom panel compares the constant density models. The optical depths at 1 μm are as indicated. The incident stellar spectrum is shown by the dashed curve. (*b*) Spherical model temperatures. Shown are the comparisons of our spherically symmetric model temperatures (*histogram*) with those from DUSTY (*solid curves*). The top panel compares the $1/r^2$ density models, while the bottom panel compares the constant density models. The optical depths at 1 μm are as indicated.

Ivezić et al. This code, called DUSTY, is publicly available[1] and is described in Ivezić & Elitzur (1997). We see that our Monte Carlo calculations reproduce both the correct temperature structure and SED. Note the large errors at the longest and shortest wavelengths in the Monte Carlo calculations. At these wavelengths, the number of emerging packets is small, resulting in large errors [the relative error in each flux bin equals $1/(N_k)^{1/2}$, owing to the Poisson sampling statistics inherent in Monte Carlo simulations]. The excellent agreement of the comparisons shown in Figures 2*a* and 2*b* (the differences are smaller than the numerical error of the DUSTY calculations) demonstrates the validity of our temperature correction procedure described in § 2.

Now that we have verified our basic radiative equilibrium algorithm, we can proceed to investigate the temperature structure and SEDs of other geometries. Owing to the inherently three-dimensional nature of Monte Carlo simulations (even our one-dimensional spherically symmetric code internally tracks the photon packets in three dimensions), our code is readily modified for arbitrary geometries. We now show the results of an application to axisymmetric circumstellar environments.

[1] The DUSTY Web site is available at http://www.pa.uky.edu/~moshe/dusty.

4. AXISYMMETRIC TWO-DIMENSIONAL CALCULATIONS

For the purpose of this illustrative simulation, we adopt a stellar blackbody with $T_* = 3500$ K, an envelope inner radius $R_{\rm dust} = 10R_*$, and a simple ellipsoidal parameterization for the circumstellar density. The isodensity contours are elliptical, with a/b being the ratio of the semimajor to semiminor axis. The density is given by

$$\rho = \rho_0 \frac{(R_{\rm dust}/r)^2}{1 + f^2 \cos^2 \theta}, \tag{21}$$

where ρ_0 is given by equation (11) ($p = 2$ case), θ is the polar angle, and the "flattening factor"

$$f = \sqrt{(a/b)^2 - 1}\,. \tag{22}$$

Note that the equatorial-to-polar density ratio at a given radius is $\rho_{\rm eq}/\rho_{\rm pole} = (a/b)^2$.

As before, we divide the circumstellar environment into cells with $N_r = 200$ radial and $N_\mu = 20$ latitudinal grid points. Note that the envelope is symmetric about the equator, so we combine the cells below the equator with their counterparts above the equator. This is automatically accomplished by using $\mu_j = \cos\theta_j$ for the latitudinal grid point coordinate. Spacing the grid so that the radial and

latitudinal optical depths are the same for each cell, we find

$$r_i = \frac{N_f}{N_f - i} R_{\rm dust} , \tag{23}$$

$$\mu_j = \frac{1}{\sqrt{1 + (a/b)^2 \tan^2 (\pi j / 2N_\mu)}} . \tag{24}$$

With these cell coordinates, equation (6) for the temperature in cell (i,j) becomes

$$T_{i,j}^4 = T_*^4 \left\{ \frac{N_{i,j}(N_f - i)(N_f - i + 1)(R_*/R_{\rm dust})^2 (1 - R_{\rm dust}/R_{\rm max}) f}{4N_\gamma \tau_V^{\rm eq} N_f [\kappa_{\rm P}(T_{i,j})/(\kappa_V + \sigma_V)][\tan^{-1}(f\mu_{j-1}) - \tan^{-1}(f\mu_j)]} \right\}, \tag{25}$$

where $N_{i,j}$ is the number of packets absorbed in the cell, and we have chosen $\lambda = 5500$ Å (V band) for our equatorial radial optical depth parameter, $\tau_V^{\rm eq}$.

For the dust opacity, we adopt a standard MRN interstellar grain mixture (Mathis, Rumpl, & Nordsieck 1977), using optical constants from Draine & Lee (1984). Figure 3 shows the opacity and albedo in graphic form. The data for this figure are available in tabular form from the DUSTY Web site.[2] Note the prominent silicate absorption features at 10 and 18 μm. For the current demonstration, we assume that the scattering is isotropic, but we can easily accommodate any phase function, analytic or tabulated, when calculating the emergent SED.

Unlike the spherically symmetric benchmarks, the SED now depends on the viewing angle, so we must bin the escaping packets in both direction and frequency. Since the envelope is axisymmetric, the observed flux only depends on the inclination angle i of the envelope symmetry axis (i.e., the stellar rotation axis). To obtain approximately equal numbers of escaping packets, we choose $N_{\rm inc} = 10$ direction bins, with equal solid angles, $\Delta\Omega = 4\pi/N_{\rm inc}$. The escaping directions (inclination angles) i_l for these bins are given by

$$\mu_l^{\rm esc} = l/N_{\rm inc} , \tag{26}$$

where $\mu_l^{\rm esc} = \cos i_l$. In addition to the direction bins, we use the frequency bins given by equation (19).

Now that we have specified both the direction and frequency bins, the observed flux is $F_{\nu_{k,l}} = N_{k,l} E_\gamma / \Delta\Omega d^2 \Delta t \Delta\nu$, where $N_{k,l}$ is the number of escaping packets in the (k,l)-bin. Normalizing to the bolometric flux F gives the emergent SED,

$$\left(\frac{\nu F_\nu}{F}\right)_{k,l} = \frac{(k - 1/2) N_{k,l} N_{\rm inc}}{N_\gamma} . \tag{27}$$

We now choose to investigate the SEDs produced by two density structures with different degrees of flattening. The first has a density ratio $\rho_{\rm eq}/\rho_{\rm pole} = 1000$ to represent a disklike structure. The second has a density ratio $\rho_{\rm eq}/\rho_{\rm pole} = 10$, which is mildly oblate, representative of an infalling protostellar envelope. For each density structure, we perform optically thick (in the mid-IR) and optically thin calculations. The optically thick calculations have an equatorial V-band optical depth $\tau_V^{\rm eq} = 200$, while the optically thin calculations have $\tau_V^{\rm eq} = 20$. Table 2 summarizes these density structures. For comparison, we also have performed calculations for $p = 2$ spherically symmetric models containing the same total mass as our disk and envelope densities. Keeping the same inner and outer radii, the optical depth for the equivalent spherical model is

$$\tau_V^{\rm sp} = \tau_V^{\rm eq} \frac{\tan^{-1} f}{f} . \tag{28}$$

4.1. *Disk Model*

Figure 4*a* shows the incident stellar spectrum and the emergent SED as a function of the viewing angle for the disklike model as well as the result of the equivalent spherically symmetric calculation. For both disk simulations, when viewing the system pole-on, we are looking through optically thin circumstellar dust (see Table 2) and can see the star at optical wavelengths. In the IR, there is an excess arising from the circumstellar disk, which reprocesses the stellar radiation. Note that, for pole-on viewing, we see the silicate features in emission since the disk is optically thin in the vertical direction. As we go to higher viewing angles, the optical depth to the central star increases, and as a result, the star becomes more extincted in the optical region. Note

[2] Available at ftp://gradj.pa.uky.edu/dusty/distribution/ism-stnd.dat.

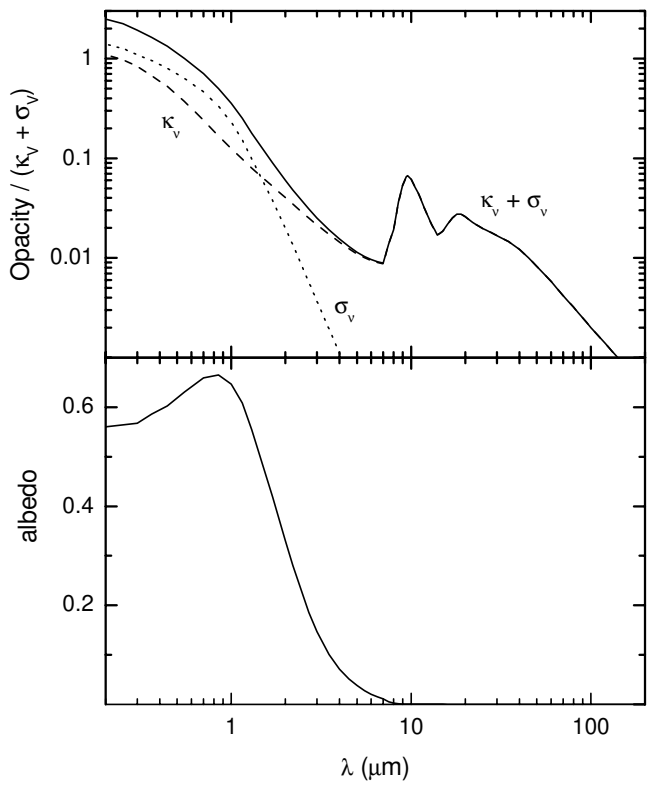

FIG. 3.—Dust opacity. The normalized absorptive (*dashed line*), scattering (*dotted line*), and total (*solid line*) opacities for the two-dimensional simulations are shown in the top panel. The bottom panel shows the corresponding albedo.

TABLE 2

ELLIPSOIDAL MODELS

$\tau_V^{\rm eq}$	$\tau_V^{\rm pole}$	$R_{\rm dust}/R_*$
$\rho_{\rm eq}/\rho_{\rm pole} = 1000$		
200.....	0.2	10
20.....	0.02	10
$\rho_{\rm eq}/\rho_{\rm pole} = 10$		
200.....	20	10
20.....	2	10

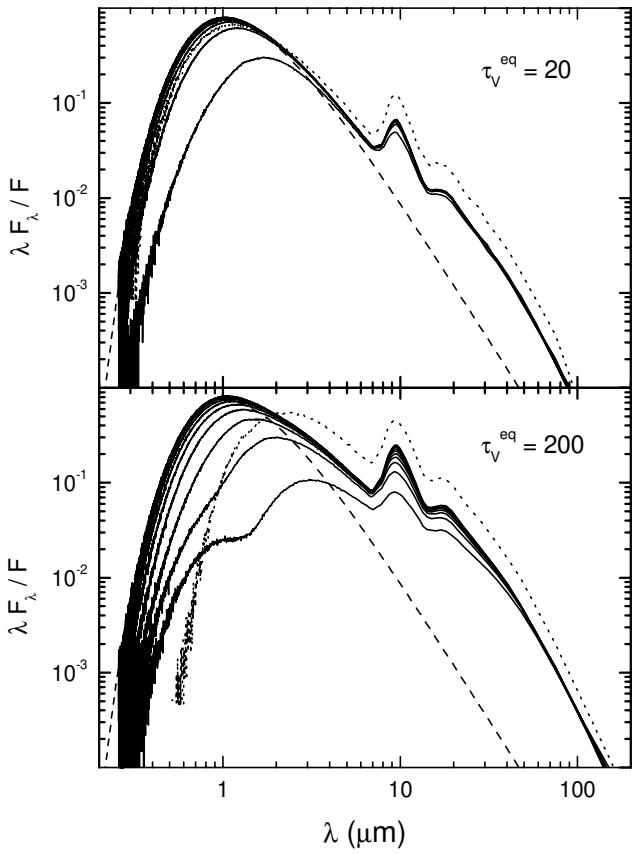

FIG. 4*a*

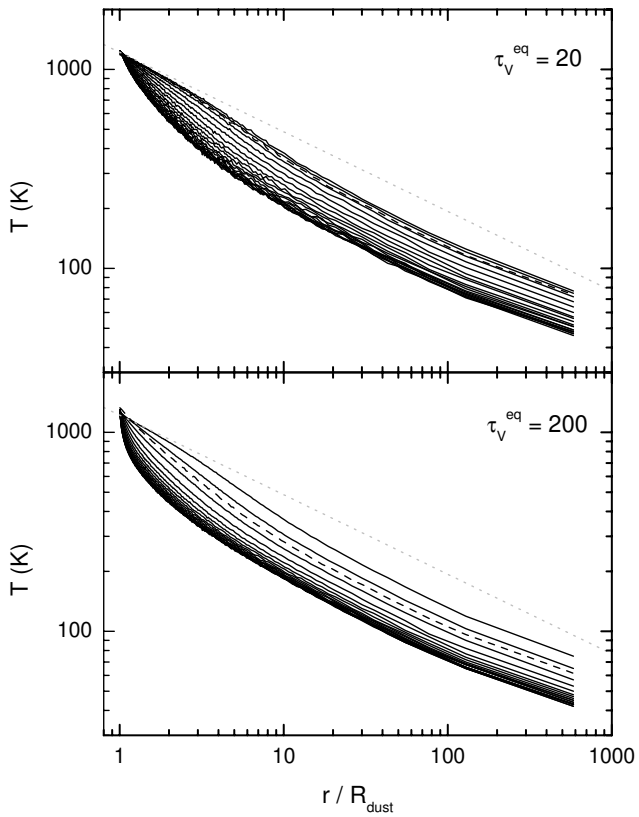

FIG. 4*b*

FIG. 4.—(*a*) Disk model SEDs. The normalized emergent fluxes (*solid lines*) are shown as a function of the viewing angle (10 inclinations, evenly spaced in cos *i*) for the disklike circumstellar density. The lowest curve corresponds to an almost edge-on view (cos $i = 0.05$), while the highest curve corresponds to an almost pole-on view (cos $i = 0.95$). The dotted curves are for a spherically symmetric simulation, having the same total circumstellar mass. The incident stellar spectrum is shown by the dashed curve. (*b*) Disk model temperatures. The temperatures (*solid lines*) are shown as a function of polar angle (20 angles, spaced as indicated in the text). The lowest curve is closest to the equatorial plane, and the highest curve is nearest to the polar axis. The dashed curve is the temperature for a spherically symmetric simulation, having the same total circumstellar mass, and the thin dotted curve is a simple power law $T \propto r^{-0.4}$ for reference.

that at almost edge-on viewing, a "shoulder" appears around 1 μm for the optically thick case. This arises because of the dominant effects of scattering the stellar radiation at these wavelengths. These scattering shoulders are also present in the axisymmetric calculations presented by Efstathiou & Rowan-Robinson (1991), Sonnhalter et al. (1995), Men'schikov & Henning (1997), and D'Alessio et al. (1999). At wavelengths longer than about 1 μm, the albedo begins to drop rapidly (see Fig. 3), and the disk thermal emission begins to dominate, so the shoulder terminates. Beyond 30 μm, the envelope becomes optically thin, so the spectrum is independent of inclination and is dominated by the dust emission.

The two-dimensional temperature structure for the disklike models is displayed in Figure 4*b*. We see that at the inner edge of the envelope ($R_{\rm dust}$), there is little variation of the temperature with latitude, while at large radii, there is a clear latitudinal temperature gradient, with the dust in the denser equatorial regions being cooler than dust at high latitudes.

In the polar region, the material is optically thin to the stellar radiation, so it heats up to the optically thin radiative equilibrium temperature. This temperature has a power-law behavior $T \propto r^{-0.4}$ for dust opacity ($\kappa \propto \lambda^{-1}$). As can be seen in Figure 4*b*, the polar temperature does indeed have a power-law decrease with a slope of approximately -0.4.

In contrast, the disk only displays this power-law behavior at large radii. At the inner edge of the disk, the disk "sees" the same mean (stellar) intensity as is present in the polar region ($J = WB$, where $W = 0.5\{1 - [1 - (R/r)^2]^{1/2}\}$ is the dilution factor). Consequently, the inner edge of the disk heats up to the optically thin radiative equilibrium temperature—the same as the polar temperature. However, at larger radii, the opaque material in the inner regions of the disk shields the outer regions from direct heating by the stellar radiation. This shielding reduces the mean intensity ($J < WB$). As a result, the outer disk is only heated to a fraction of the optically thin radiative equilibrium temperature. Thus, the equatorial region is cooler than the polar region. Eventually, at large enough radii, the disk becomes optically thin to the heating radiation. At that point, it sees a radially streaming radiation field from an effective photosphere that has a much lower temperature than the star. From that point outward, the disk temperature displays an optically thin power-law decrease with a slope that parallels the polar temperature.

The spherically symmetric calculation overestimates both the emergent flux and the disk temperature. In the optically thin limit, the IR continuum is proportional to the mass of the circumstellar material, so one would expect that a spherically equivalent mass would reproduce the long-wavelength spectrum. Recall, however, that we can see the

star at pole-on viewing angles. This implies that the disk does not reprocess the entire bolometric luminosity of the star. Consequently, the IR excess is less than that in the spherical model. Note that one can nonetheless reproduce the edge-on SED using a spherical model if we allow the density power law to depart from $1/r^2$ and change the size of the spherical envelope. This also was noted by Sonnhalter et al. (1995), who found that they could fit the IR continuum of their disk models by changing the radial dependence of the circumstellar density and the outer radius for the same total envelope mass.

4.2. *Envelope Model*

The SED and temperature structure for the oblate envelope are shown in Figures 5*a* and 5*b*. The optically thin envelope displays significant extinction of the star at all viewing angles. Close to edge-on, scattering shoulders appear around 1 μm that are similar to those seen in the disk model (Fig. 4*a*). Finally, because the model is optically thin in the mid-IR, the silicate feature is always in emission, and the SED is independent of the viewing angle for wavelengths longer than a few microns.

For the denser envelope, the star is extremely faint at optical wavelengths. Along with the increased extinction in the optical, the scattering shoulders are less prominent because of the thermal emission by the envelope. In the mid-IR, the envelope is optically thick edge-on and optically thin pole-on. Consequently, the silicate features go from absorption to emission as the viewing angle changes from edge-on to pole-on. The general shape of the SEDs, which now peak in the mid-IR for all inclinations, are reminiscent of spectra from embedded (class I) T Tauri stars, which are commonly modeled using flattened axisymmetric dusty envelopes (e.g., Adams, Lada, & Shu 1987; Kenyon, Calvet, & Hartmann 1993; Men'shchikov & Henning 1997; D'Alessio, Calvet, & Hartmann 1997). Of these T Tauri simulations, only Efstathiou & Rowan-Robinson (1991) have performed an exact calculation for the SED and circumstellar temperature for the Terebey, Shu, & Cassen (1984) collapse model.

The temperature structure for our envelope models (Fig. 5*b*) is qualitatively similar to the temperature structure of the disk models (Fig. 4*b*). The temperature at the inner edge of the envelope is independent of latitude, while at larger radii, the equatorial regions are cooler than the polar regions. The primary difference is that the latitudinal temperature gradient is not as extreme.

Finally, we note that the equivalent spherically symmetric model better reproduces the far-IR spectrum of the envelope models than the disk models. This is because the envelope models reprocess the entire bolometric luminosity, while in disk models, some of the stellar luminosity escapes through the polar region.

5. DISCUSSION

We have developed a temperature correction procedure for use in Monte Carlo radiation transfer codes. We have tested our method against other spherically symmetric benchmark codes and successfully matched their results. After verifying our method, we applied it to obtain sample

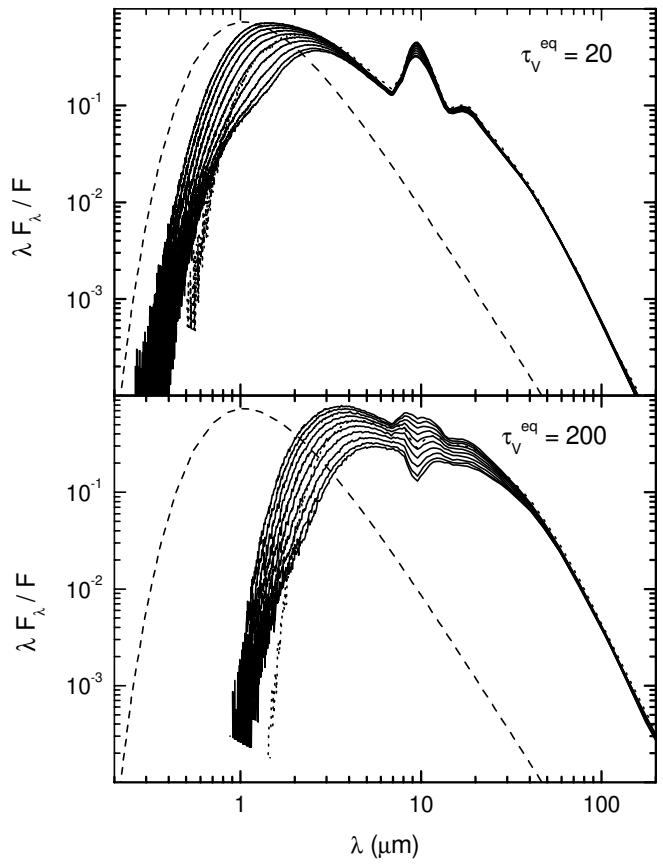

FIG. 5*a*

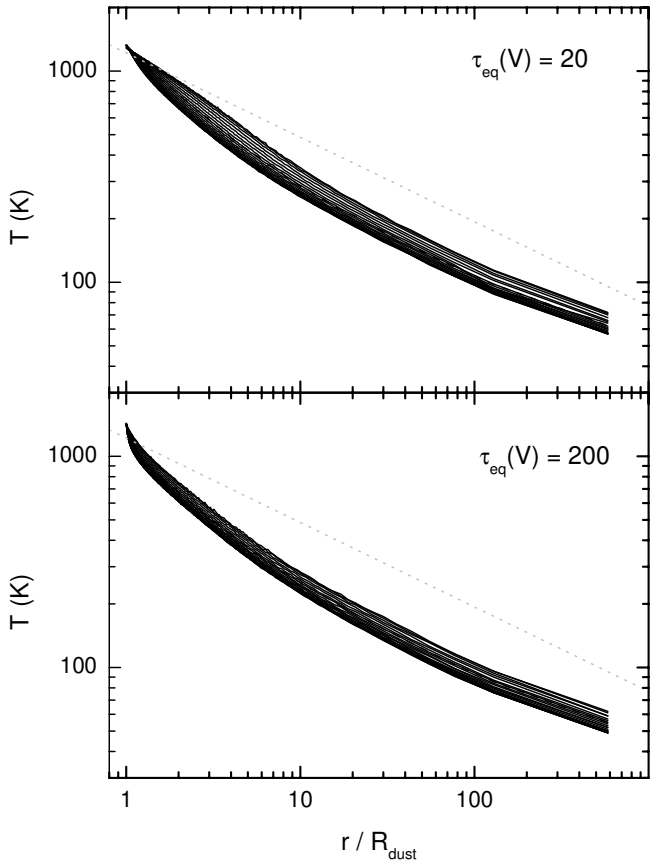

FIG. 5*b*

FIG. 5.—(*a*) Envelope model SEDs. Same as Fig. 4*a*, but for the envelope density distribution. (*b*) Envelope model temperatures. Same as Fig. 4*b*, but for the envelope density distribution.

temperature distributions and SEDs for two-dimensional axisymmetric disklike models and mildly oblate envelopes. These simulations illustrate the important role envelope geometry can play when interpreting the SEDs of embedded sources.

The primary limitation of our temperature correction procedure is that it only applies if the opacity is independent of temperature. This is not true for free-free opacity or hydrogen bound-free opacity, but it is true for dust opacity, which is the dominant opacity source in many astrophysical situations. The reason our method is limited to temperature-independent opacities is that two associated problems occur if the opacity varies when the cell's temperature changes. The first is that the cell will have absorbed either too many or too few of the previous packets passing through the cell. The second is the associated change in the interaction locations of the previous packets, which implies that the paths of the previous photon packets should have been different. These problems do not occur if the opacity is independent of temperature.

Lucy (1999) has proposed a slightly different method to calculate the equilibrium temperature. Instead of sampling photon absorption, he directly samples the photon density (equivalent to the mean intensity) by summing the path length of all packets that pass through a cell. Typically, more packets pass through a cell than are absorbed in the cell, so this method potentially produces a more accurate measurement of the temperature for a given total number of packets, especially when the envelope is very optically thin. The disadvantage of his method is that it requires iteration to determine the envelope temperature. In principle, one could partially combine both methods. First, run our simulation, adding path length counters to each cell. After running all packets, use the path length information to calculate a final temperature. This will provide a more accurate temperature that can be used to calculate the source function. After obtaining the source function for each cell, it is a simple matter to integrate the transfer equation to obtain the SED.

Another limitation of the Monte Carlo method is that it is not well suited to envelopes with very high optical depths ($\tau > 100$–1000), unless there is an escape channel for the photons. For example, geometrically thin disks can be extremely optically thick in the radial direction, but optically thin in the polar direction, providing an escape channel for the photons. Similarly, dense envelopes can be very optically thick to the illumination source, but optically thin to the reprocessed radiation, which is a another escape channel. In the event that no such escape channels exist, one must turn to other methods. We are currently investigating how to couple the Monte Carlo simulation in the optically thinner regions with other methods in the optically thick interior.

The focus of the present paper has been on the development and implementation of the temperature correction procedure. For this reason, we have made several simplifying assumptions regarding the circumstellar opacity and geometry. For example, we have assumed a single temperature for all dust grains regardless of their size and composition. This differs from other investigations in which different types of grains can have different temperatures at the same spatial location (e.g., the spherically symmetric radiation transfer code developed by Wolfire & Cassinelli 1986). Similarly, we have not implemented a procedure to solve for the location of the dust destruction radius, which will be different for grains of differing size and composition. These issues are currently under investigation.

With the speed of today's computers, Monte Carlo radiation transfer simulations can be performed in a reasonably short time. The two-dimensional simulations presented in this paper employed 10^8 packets, requiring about 2 hr of CPU time; the spherically symmetric cases used 10^6 packets, requiring about 1 minute. So for continuum transfer, Monte Carlo simulation is proving to be a very powerful technique for investigating arbitrary density structures and illuminations.

We would like to thank Barbara Whitney and Mário Magalhães for many discussions relating to this work. An anonymous referee also provided thoughtful comments that helped improve the clarity of our presentation. This work has been funded by NASA grants NAG 5-3248 and NAG 5-6039 and NSF grant AST 98-19928.

REFERENCES

Adams, F. C., Lada, C. J., & Shu, F. H. 1987, ApJ, 312, 788
Carter, L. L., & Cashwell, E. D. 1975, Particle Transport Simulation with the Monte Carlo Method (Oak Ridge: ERDA)
Code, A. D., & Whitney, B. A. 1995, ApJ, 441, 400
D'Alessio, P., Calvet, N., & Hartmann, L. 1997, ApJ, 474, 397
D'Alessio, P., Calvet, N., Hartmann, L., Lizano, S., & Cantó, J. 1999, ApJ, 527, 893
Draine, B. T., & Lee, H. M. 1984, ApJ, 285, 89
Efstathiou, A., & Rowan-Robinson, M. 1990, MNRAS, 245, 275
———. 1991, MNRAS, 252, 528
Ivezić, Ž., & Elitzur, M. 1997, MNRAS, 287, 799
Ivezić, Ž., Groenewegen, M. A. T., Men'shchikov, A., & Szczerba, R. 1997, MNRAS, 291, 121
Kenyon, S. J., Calvet, N., & Hartmann, L. 1993, ApJ, 414, 676
Lefevre, J., Bergeat, J., & Daniel, J. Y. 1982, A&A, 114, 341
Lefevre, J., Daniel, J. Y., & Bergeat, J. 1983, A&A, 121, 51
Leung, C. M. 1976, ApJ, 209, 75
Lucy, L. B. 1999, A&A, 344, 282
Mathis, J. S., Rumpl, W., & Nordsieck, K. H. 1977, ApJ, 217, 425
Men'shchikov, A. B., & Henning, T. 1997, A&A, 318, 879
Rowan-Robinson, M. 1980, ApJS, 44, 403
Scoville, N. Z., & Kwan, J. 1976, ApJ, 206, 718
Sonnhalter, C., Preibisch, T., & Yorke, H. W. 1995, A&A, 299, 545
Terebey, S., Shu, F. H., & Cassen, P. 1984, ApJ, 286, 529
Whitney, B. A., & Hartmann, L. 1992, ApJ, 395, 529
———. 1993, ApJ, 402, 605
Wolf, S., Henning, Th., & Secklum, B. 1999, A&A, 349, 839
Wolfire, M. G., & Cassinelli, J. P. 1986, ApJ, 310, 207
Wood, K., Bjorkman, J. E., Whitney, B. A., & Code, A. D. 1996, ApJ, 461, 828
Yorke, H. W. 1980, A&A, 86, 286